

光学学报

1064 nm 高功率明亮压缩态光场制备实验中绿光诱导红外吸收效应

郭锐¹, 杨文海^{2*}, 郭咏¹, 姚慧¹

¹山西农业大学物理系, 山西 太谷 030801;

²中国空间技术研究院西安分院, 陕西 西安 710000

摘要 通过实验和理论研究连续变量高功率明亮压缩态光场制备实验中高功率种子光注入光学参量放大器引起的绿光诱导红外吸收效应。首先, 通过优化实验系统工作参数, 提升反馈控制回路的锁定稳定性, 当种子光功率为 500 mW、泵浦光功率为 145 mW 时, 在分析频率为 3 MHz 处, 获得光功率为 200 μW、压缩度为 (-10.7 ± 0.2) dB 的明亮压缩态光场。然后, 根据实验数据, 定量分析高功率明亮压缩态光场与压缩真空态光场产生过程中周期极化磷酸氧钛钾晶体的吸收损耗, 发现高功率明亮压缩态光场实验系统的总光学损耗为 (9 ± 0.05) %, 其中由周期极化磷酸氧钛钾晶体吸收导致的内腔损耗为 (5.8 ± 0.05) %, 占总光学损耗的 (64.4 ± 0.05) %。该条件下周期极化磷酸氧钛钾晶体对高功率明亮压缩态光场的吸收系数为 $(6.0 \pm 0.05) \times 10^{-2} \text{ cm}^{-1}$ 。当泵浦光单独注入光学参量放大器时, 周期极化磷酸氧钛钾晶体对压缩真空态光场的吸收系数约为 $2.1 \times 10^{-4} \text{ cm}^{-1}$ 。由此可知, 当高功率种子光注入光学参量放大器时, 绿光诱导红外吸收效应使周期极化磷酸氧钛钾晶体的吸收系数增加了 285 倍, 使内腔损耗成为高功率明亮压缩态光场压缩度的主要影响因素。

关键词 量子光学; 明亮压缩态光场; 绿光诱导红外吸收效应; 内腔损耗

中图分类号 O436

文献标志码 A

DOI: 10.3788/AOS222031

1 引言

连续变量压缩态光场作为一种重要的非经典光场^[1-2], 可以抑制部分相干态光场的量子噪声, 提高光学信号的信噪比和成像分辨率, 使光学系统获得超越标准量子极限的探测灵敏度^[3-5]或突破夫琅禾费衍射极限的角分辨率^[6-7]。根据光场的平均振幅, 连续变量压缩态光场可分为压缩真空态光场和明亮压缩态光场。压缩真空态光场的平均振幅为零, 而明亮压缩态光场的平均振幅大于零。基于以上两类连续变量压缩态光场的不同特性, 其应用场景不同, 如: 压缩真空态光场可注入激光干涉仪, 降低干涉仪输出信号的强度噪声或相位噪声^[8-9]; 明亮压缩态光场可用于量子增强激光雷达^[10]和磁力计^[11], 以及量子密集编码、量子密钥分发和离物传态^[12-16]。

基于二阶非线性光学效应的参量下转换过程是目前制备连续变量压缩态光场最有效的方法之一。国际上以引力波探测项目为牵引, 针对连续变量压缩态光场的研究主要聚焦于压缩真空态光场的实验制备^[7, 17]。国内开展连续变量压缩态光场研究的单位较少, 其中以山西大学为代表, 已经制出 -12.6 dB 的明亮压缩

态光场和 -13.8 dB 的压缩真空态光场^[18-19]。本文首先从光学参量放大器(OPA)的内腔损耗和逃逸效率出发, 搭建了一套产生高功率明亮压缩态光场的实验系统, 通过增大注入 OPA 的种子光功率、优化泵浦光功率, 实现了光功率为 200 μW, 压缩度为 (-10.7 ± 0.2) dB 的高功率明亮压缩态光场的稳定输出。然后, 根据实验数据和理论计算结果, 定量分析了高功率明亮压缩态光场与压缩真空态光场产生过程中周期极化磷酸氧钛钾(PPKTP)晶体对 1064 nm 压缩态光场的吸收系数。

2 实验系统

图 1 所示为制备连续变量高功率明亮压缩态光场的实验系统。实验系统的基频光源采用山西大学光电研究所研制的高功率 1064 nm 单频 Nd: YVO₄ 固体激光器; 二次谐波光源采用基于掺氧化镁的铌酸锂(MgO: LiNbO₃)晶体的平凹型半整块倍频腔, 通过临界相位匹配技术倍频获得 532 nm 激光^[20-21]。实验系统的核心部分为产生连续变量高功率明亮压缩态光场的 OPA, 其基于 PPKTP 晶体和一片凹面腔镜构成半整块驻波腔。在实验系统的平衡零拍探测部分, 将本底

收稿日期: 2022-11-22; 修回日期: 2022-12-05; 录用日期: 2023-01-03; 网络首发日期: 2023-02-07

基金项目: 国家自然科学基金(62001374)

通信作者: *yangwh1@cast504.com

光和信号光在50/50分束器上均分并在干涉后注入平衡零拍探测器,通过扫描本底光和信号光的相对相位实现明亮压缩态光场噪声功率谱的测量。为了优化实验系统中各部分高斯光束的空间模式分布,提升高斯光束与光学谐振腔的模式匹配效率,并降低光场携带的相对强度噪声和相位噪声,在实验系统基频光路、二

次谐波光路和平衡零拍探测部分的本底光路中插入基于三镜环形腔的模式清洁器。此外,在上述连续变量高功率明亮压缩态光场制备实验系统中,所有光学谐振腔和光场相对相位的锁定均采用Pound-Drever-Hall(PDH)技术实现。

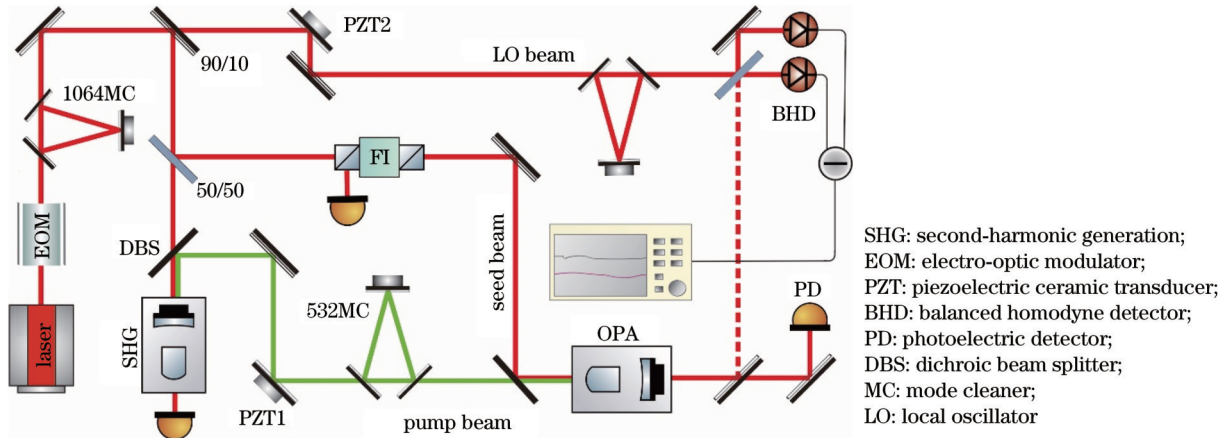


图1 连续变量高功率明亮压缩态光场实验系统

Fig. 1 Experimental system of continuous variable high-power bright squeezed light field

3 实验过程与结果

连续变量高功率明亮压缩态光场的实验制备过程如下:将高功率1064 nm单频Nd:YVO₄固体激光器输出的激光光场注入模式清洁器,在优化空间模式分布后,经90/10分束器分为两束,其中一束作为本底光注入平衡零拍探测器放大压缩态光场的噪声功率;另一束经50/50分束器分为光功率相等的两部分,其中一部分作为基频光注入倍频腔,产生用于泵浦OPA的二次谐波光场,另一部分作为种子光注入OPA,用于产生明亮压缩态光场。

为了获得高功率明亮压缩态光场,需要提高注入OPA的种子光功率。高功率种子光注入OPA会导致PPKTP晶体对1064 nm压缩态光场的吸收迅速增加,从而引起严重的热效应,给泵浦光场和种子光场相对相位的精确锁定及OPA腔长的稳定控制带来了巨大的挑战。因此,通过优化OPA驻波腔的结构和参数^[21-23],引入电光相位调制器非线性晶体后端面楔角^[24-25],改进光电探测器的电路设计^[26],从而提升OPA在高功率种子光注入情况下的PDH反馈控制环路的稳定性和锁定精度,为获得高功率的明亮压缩态光场提供技术支持。

为了制备高功率明亮压缩态光场,采用有利于产生宽频带压缩态光场的双凹型半整块驻波腔^[21-22],并优化OPA的主要参数,具体参数如下:几何腔长为35 mm,PPKTP晶体的尺寸为1 mm×2 mm×10 mm,前端凸面曲率半径为12 mm,并镀有532 nm减反膜和1064 nm高反膜,位于腔内的后端平面镀有532 nm和

1064 nm双波长减反膜;输出耦合镜的曲率半径为30 mm,镀有透射率为12%的1064 nm部分反射膜和532 nm高反膜。通过上述参数可以计算得出OPA的线宽为70.7 MHz。通过实验可测得OPA的阈值为228 mW。当种子光功率为500 mW、泵浦功率为145 mW时,在分析频率为3 MHz处,测得OPA输出的明亮压缩态光场的光功率为200 μW,压缩度为(-10.7 ± 0.2) dB,如图2所示,其中 f_{RBW} 为分辨率带宽, f_{VBW} 为视频带宽。继续增大种子光功率,OPA腔长的锁定、泵浦光和种子光相对相位的锁定恶化,平衡零拍探测器饱和效应加剧,导致OPA输出的明亮压缩态光场各项指标急剧恶化。由此可知,OPA可以稳定输出明亮压缩态光场的最高功率为200 μW。OPA输入端,即PPKTP晶体前端凸面所镀1064 nm高反膜对种子光的透过率约为0.05%,当种子光功率为500 mW时,约有250 μW种子光可透过1064 nm高反膜注入OPA与泵浦光相互作用。根据OPA输出耦合镜的透射率和OPA输出明亮压缩态光场的功率,可以反推出OPA腔内经PPKTP晶体参量放大和谐振腔增强过程产生的高功率明亮压缩态光场的光功率约为1.67 mW。

OPA输出明亮压缩态光场的噪声功率谱公式为

$$V_{\text{as}} = 1 \pm \frac{4(1 - l_{\text{tot}})\sqrt{P_{\text{sh}}/P_{\text{th}}}}{\left(1 \mp \sqrt{P_{\text{sh}}/P_{\text{th}}}\right)^2 + 4(f/\kappa)^2}, \quad (1)$$

式中: P_{sh} 为泵浦功率; P_{th} 为OPA阈值; f 为分析频率; κ 为OPA线宽。将OPA相关参数代入式(1)可以得到OPA输出明亮压缩态光场压缩度随分析频率的变化

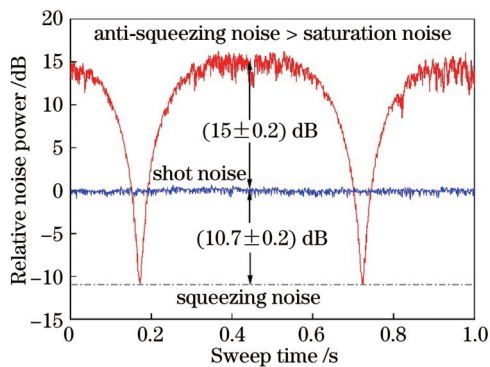


图2 分析频率为3 MHz ($f_{\text{RBW}}=300 \text{ kHz}$, $f_{\text{VBW}}=200 \text{ Hz}$)时高功率明亮压缩态光场的噪声功率谱

Fig. 2 Noise power spectrum of high-power bright squeezed light field at analysis frequency of 3 MHz ($f_{\text{RBW}}=300 \text{ kHz}$, $f_{\text{VBW}}=200 \text{ Hz}$)

曲线,如图3所示。由图3可知,当分析频率小于3 MHz时,OPA输出明亮压缩态光场的压缩度几乎不会受到OPA线宽的影响。

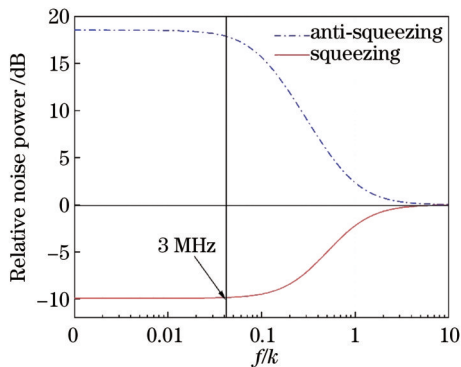


图3 OPA输出明亮压缩态光场压缩度随分析频率的变化趋势

Fig. 3 Compressibility of OPA bright squeezed light field changed with analysis frequency

图2所示的明亮压缩态光场的反压缩度明显低于图3所示的理论计算的反压缩度,这主要是因为反压缩噪声曲线中出现大幅度无规则噪声。高功率明亮压缩态光场与本底光干涉相长后光功率太大,平衡零拍探测器内部电路自激和运算放大器饱和,由此产生上述无规则噪声。平衡零拍探测器饱和后输出的噪声功率信号已经失真,无法准确测量明亮压缩态光场的反压缩噪声功率,因此图2的反压缩噪声功率其实是平衡零拍探测器的饱和噪声功率。

根据上述实验数据和理论计算结果,OPA产生的明亮压缩态光场传输到平衡零拍探测器,产生的总光学损耗为(9±0.05)%。由实验系统光路结构可知,总光学损耗包括高功率明亮压缩态光场产生过程中OPA的内腔损耗、明亮压缩态光场传输过程中经过光学元件表面和基底材料引入的光学损耗,以及平衡零拍探测器光电二极管量子效率不理想引入的损耗。其

中传输损耗可以通过光学元件生产厂家给出的镀膜参数估算。在本实验系统中,明亮压缩态光场传输经过的光学器件依次为OPA输出腔镜、准直透镜、导光镜、50/50分束器、平衡零拍两臂光路导光镜、聚焦透镜和光电二极管保护窗片,由生产厂家给出的镀膜参数可知,总传输损耗为(2±0.05)%。平衡零拍探测器使用的光电二极管量子效率标称值大于99%,引入的光学损耗小于1%。根据以上数据可以估算出OPA的内腔损耗为(6±0.05)%。OPA逃逸效率的计算公式为

$$\eta = T/(T+L), \quad (2)$$

式中:T为OPA输出腔镜的透射率;L为OPA的内腔损耗。将上述参数代入式(2)可计算出本实验条件下OPA的逃逸效率为(66.7±0.05)%。此值与文献[27]中OPA的逃逸效率98.34%相差较大。对比文献[27]与本实验系统的工作参数可知,高功率种子光注入OPA是本实验系统与文献[27]实验系统的最大区别。由此可以初步判断高功率种子光注入是OPA内腔损耗增加和逃逸效率降低的主要影响因素。为了验证上述结论,分析了高功率明亮压缩态光场制备过程中可能对压缩度产生不利影响的主要因素。经分析得知OPA的内腔损耗主要由腔镜和PPKTP晶体端面镀膜不完美以及PPKTP晶体吸收产生,由厂家给出的腔镜和PPKTP晶体端面镀膜参数可知,由腔镜和PPKTP晶体端面镀膜不完美引入的损耗约为0.2%,由此可以计算出在泵浦光功率为145 mW、种子光功率为500 mW的条件下,PPKTP晶体的吸收损耗为(5.8±0.05)%占总光学损耗的(64.4±0.05)%。由上述理论计算结果可知,高功率种子光注入OPA导致PPKTP晶体吸收损耗显著增加,PPKTP晶体的吸收损耗超过腔镜和PPKTP晶体端面镀膜不完美引入的损耗,成为内腔损耗的主要来源。

根据布朗-朗伯定律($I=I_0 e^{-al}$,其中 I_0 表示入射光强, I 表示光经过介质后的出射光强, l 为介质长度, α 为介质吸收系数),可以算出该条件下PPKTP晶体的吸收系数约为 $6.0 \times 10^{-2} \text{ cm}^{-1}$ 。而根据文献[27],在泵浦光(功率为145 mW)单独注入OPA时,PPKTP晶体的吸收系数约为 $2.1 \times 10^{-4} \text{ cm}^{-1}$,是本实验系统在高功率种子光注入OPA时晶体吸收系数的1/286。由此可知,高功率种子光注入OPA导致PPKTP晶体对1064 nm高功率明亮压缩态光场的吸收系数大幅度增加。根据文献[28]给出的理论模型,高功率泵浦光注入OPA导致PPKTP晶体产生灰迹效应,即浅势阱内产生大量空穴^[29]。在文献[27]的实验条件下,OPA腔内的压缩真空光功率极低,使PPKTP晶体浅势阱内空穴的消耗速率小于产生速率;在本实验制备高功率明亮压缩态光场的条件下,OPA腔内的明亮压缩态光场的光功率约为1.67 mW,使PPKTP晶体浅势阱内空穴的消耗速率显著提升,即PPKTP晶体对明亮压

缩态光场的吸收系数大幅增加。由此可知,PPKTP晶体内部产生了剧烈的绿光诱导红外吸收(GLIIRA)效应。

4 结 论

通过实验和理论研究了连续变量高功率明亮压缩态光场制备实验中,高功率种子光注入OPA条件下PPKTP晶体内部的GLIIRA效应。首先,通过优化实验系统工作参数,提升PDH反馈控制回路在高功率种子光注入OPA状态下的锁定精度和稳定性,当种子光功率为500 mW、泵浦光功率为145 mW时,在分析频率3 MHz处,获得光功率为200 μ W、压缩度为(-10.7 ± 0.2) dB的明亮压缩态光场。然后,根据实验数据和理论计算结果,本实验系统中高功率明亮压缩态光场从产生到探测引入的总光学损耗为(9 \pm 0.05)% ,其中OPA的内腔损耗为(6 \pm 0.05)% ,GLIIRA效应产生的吸收损耗为(5.8 \pm 0.05)% ,占总光学损耗的(64.4 \pm 0.05)% 。该研究结果证实了高功率明亮压缩态光场实验产生系统在高功率种子光注入OPA时,PPKTP晶体内部的GLIIRA效应加剧,使PPKTP晶体的吸收损耗成为内腔损耗的主要来源,致使吸收损耗成为明亮压缩态光场压缩度的主要影响因素。本研究的结论指出了现阶段实验制备高功率明亮压缩态光场存在的技术难题,为下一步研制功率更高、压缩度更大和输出指标更加稳定的明亮压缩态光场指明了方向。

参 考 文 献

- [1] Braunstein S L, van Loock P. Quantum information with continuous variables[J]. *Reviews of Modern Physics*, 2005, 77(2): 513-577.
- [2] Furusawa A, Sorensen J L, Braunstein S L, et al. Unconditional quantum teleportation[J]. *Science*, 1998, 282(5389): 706-709.
- [3] 史少平, 杨文海, 郑耀辉, 等. 压缩态光场制备中的单频激光源噪声分析[J]. 中国激光, 2019, 46(7): 0701009.
Shi S P, Yang W H, Zheng Y H, et al. Noise analysis of single-frequency laser source in preparation of squeezed-state light field [J]. *Chinese Journal of Lasers*, 2019, 46(7): 0701009.
- [4] 杨鹏, 柯学志, 张风雷, 等. 亚散粒噪声亚赫兹激光干涉测量研究[J]. 激光与光电子学进展, 2022, 59(1): 0127001.
Yang P, Ke X Z, Zhang F L, et al. Sub-shot-noise sub-hertz laser-interferometric measurement[J]. *Laser & Optoelectronics Progress*, 2022, 59(1): 0127001.
- [5] Yu X D, Li W, Zhu S Y, et al. Mach-Zehnder interferometer with squeezed and EPR entangled optical fields[J]. *Chinese Physics B*, 2016, 25(2): 020304.
- [6] Taylor M A, Janousek J, Daria V, et al. Biological measurement beyond the quantum limit[J]. *Nature Photonics*, 2013, 7: 229-233.
- [7] Taylor M A, Janousek J, Daria V, et al. Subdiffraction-limited quantum imaging within a living cell[J]. *Physical Review X*, 2014, 4(1): 011017.
- [8] Tse M, Yu H C, Kijbunchoo N, et al. Quantum-enhanced advanced LIGO detectors in the era of gravitational-wave astronomy[J]. *Physical Review Letters*, 2019, 123(23): 231107.
- [9] 刘翊钊, 左小杰, 同智辉, 等. 基于光学参量放大器的量子干涉仪的分析[J]. 光学学报, 2022, 42(3): 0327013.
Liu Y Z, Zuo X J, Yan Z H, et al. Analysis of quantum interferometer based on optical parametric amplifier[J]. *Acta Optica Sinica*, 2022, 42(3): 0327013.
- [10] Dutton Z, Shapiro J H, Guha S. LADAR resolution improvement using receivers enhanced with squeezed-vacuum injection and phase-sensitive amplification[J]. *Journal of the Optical Society of America B*, 2010, 27(6): A63-A72.
- [11] Li B B, Bílek J, Hoff U B, et al. Quantum-enhanced optomechanical magnetometry[J]. *Optica*, 2018, 5(7): 850-856.
- [12] Gottesman D, Kitaev A, Preskill J. Encoding a qubit in an oscillator[J]. *Physical Review A*, 2001, 64(1): 012310.
- [13] 刘涛, 朱聪, 孙春阳, 等. 不同天气条件对自由空间量子通信系统性能的影响[J]. 光学学报, 2020, 40(2): 0227001.
Liu T, Zhu C, Sun C Y, et al. Influences of different weather conditions on performance of free-space quantum communication system[J]. *Acta Optica Sinica*, 2020, 40(2): 0227001.
- [14] Kaiser F, Fedrici B, Zavatta A, et al. A fully guided-wave squeezing experiment for fiber quantum networks[J]. *Optica*, 2016, 3(4): 362-365.
- [15] Wu Y M, Wang Q W, Tian L, et al. Multi-channel multiplexing quantum teleportation based on the entangled sideband modes[J]. *Photonics Research*, 2022, 10(8): 1909-1914.
- [16] Shi S P, Tian L, Wang Y J, et al. Demonstration of channel multiplexing quantum communication exploiting entangled sideband modes[J]. *Physical Review Letters*, 2020, 125(7): 070502.
- [17] Vahlbruch H, Mehmet M, Danzmann K, et al. Detection of 15 dB squeezed states of light and their application for the absolute calibration of photoelectric quantum efficiency[J]. *Physical Review Letters*, 2016, 117(11): 110801.
- [18] Yang W H, Shi S P, Wang Y J, et al. Detection of stably bright squeezed light with the quantum noise reduction of 12.6 dB by mutually compensating the phase fluctuations[J]. *Optics Letters*, 2017, 42(21): 4553-4556.
- [19] Sun X C, Wang Y J, Tian L, et al. Detection of 13.8 dB squeezed vacuum states by optimizing the interference efficiency and gain of balanced homodyne detection[J]. *Chinese Optics Letters*, 2019, 17(7): 072701.
- [20] 田宇航, 王俊萍, 杨文海, 等. 集成量子压缩光源中MgO:LiNbO₃晶体倍频系统研究[J]. 中国激光, 2020, 47(11): 1108001.
Tian Y H, Wang J P, Yang W H, et al. Frequency doubling system for integrated quantum squeezed light source based on MgO: LiNbO₃ crystal[J]. *Chinese Journal of Lasers*, 2020, 47(11): 1108001.
- [21] 张晓莉, 王庆伟, 姚文秀, 等. 热透镜效应对半整块腔型中二次谐波过程的影响[J]. 物理学报, 2022, 71(18): 184203.
Zhang X L, Wang Q W, Yao W X, et al. Influence of thermal lens effect on second harmonic process in semi-monolithic cavity scheme[J]. *Acta Physica Sinica*, 2022, 71(18): 184203.
- [22] 王俊萍, 张文慧, 李瑞鑫, 等. 宽频带压缩态光场光学参量腔的设计[J]. 物理学报, 2020, 69(23): 234204.
Wang J P, Zhang W H, Li R X, et al. Design of optical parametric cavity for broadband squeezed light field[J]. *Acta Physica Sinica*, 2020, 69(23): 234204.
- [23] 郑耀辉, 张文慧, 彭塑墀. 光学谐振腔: CN108462029B[P]. 2021-03-30.
Zheng Y H, Zhang W H, Peng S C. Optical resonator: CN108462029B[P]. 2021-03-30.
- [24] Li Z X, Tian Y H, Wang Y J, et al. Residual amplitude modulation and its mitigation in wedged electro-optic modulator [J]. *Optics Express*, 2019, 27(5): 7064-7071.
- [25] Li Z X, Ma W G, Yang W H, et al. Reduction of zero baseline drift of the Pound-Drever-Hall error signal with a wedged

- electro-optical crystal for squeezed state generation[J]. Optics Letters, 2016, 41(14): 3331-3334.
- [26] Wang J R, Wang Q W, Tian L, et al. A low-noise, high-SNR balanced homodyne detector for the bright squeezed state measurement in 1-100 kHz range[J]. Chinese Physics B, 2020, 29(3): 034205.
- [27] Shi S P, Wang Y J, Yang W H, et al. Detection and perfect fitting of 13.2 dB squeezed vacuum states by considering green-light-induced infrared absorption[J]. Optics Letters, 2018, 43(21): 5411-5414.
- [28] Mabuchi H, Polzik E S, Kimble H J. Blue-light-induced infrared absorption in KNbO₃[J]. Journal of the Optical Society of America B, 1994, 11(10): 2023-2029.
- [29] Wang S, Pasiskevicius V, Laurell F. Dynamics of green-light induced infrared absorption in KTiOPO₄ and periodically poled KTiOPO₄[J]. Journal of Applied Physics, 2004, 96(4): 2023-2028.

Green Light-Induced Infrared Absorption Effect in Preparation Experiment of High-Power Bright Squeezed State Light Field of 1064 nm

Guo Rui¹, Yang Wenhui^{2*}, Guo Yong¹, Yao Hui¹

¹Department of Physics, Shanxi Agricultural University, Taigu 030801, Shanxi, China;

²China Academy of Space Technology (Xi'an), Xi'an 710000, Shaanxi, China

Abstract

Objective Continuous variable bright squeezed state light field is a very important quantum resource. It can be used in various domains such as quantum metrology, quantum precision measurement, and quantum information. Examples include quantum-enhanced lidars, magnetometers, quantum-dense coding, quantum key distribution, and teleportation. Applications in these domains require continuous variable bright squeezed state light fields with relatively high power. In order to obtain a continuous variable high-power bright squeezed state light field, the main factors affecting the intensity of green light-induced infrared absorption in a nonlinear periodically poled KTiOPO₄ (PPKTP) crystal are studied in the process of parametric down conversion technique. Through the research on this manuscript, one of the main factors limiting the experimental preparation of continuous variable high-power bright squeezed state light field is found, which lays a foundation for overcoming the technical problem and developing continuous variable high-power bright squeezed state lights.

Methods The experimental preparation system of continuous variable high-power bright squeezed state light field is shown in Fig. 1. The first part is the fundamental frequency light source of the experimental system, which is a high-power single-frequency Nd:YVO₄ solid-state laser of 1064 nm. The second harmonic source is a flat-concave semi-monolithic standing cavity based on MgO:LiNbO₃ crystal. The laser of 532 nm is obtained by a critical phase-matching technique in the nonlinear crystal. The second part is the core part of the experimental system, namely the optical parametric amplifier. It generates a continuous variable high-power bright squeezed state light field and is based on a semi-monolithic standing cavity composed of PPKTP crystal and a concave cavity mirror. The last part is the balanced homodyne detection part of the experimental system. The local oscillator and signal light are evenly divided and interfered on the 50/50 beam splitter and then injected into the balanced homodyne detector. The noise power spectrum of the bright squeezed optical field is measured by scanning the relative phase of the local oscillator and the signal light. In order to optimize the spatial mode distribution of the Gaussian beam in each part of the experimental system, improve the mode matching efficiency between the Gaussian beam and optical resonant cavity, and reduce the relative intensity noise and phase noise carried by the light field, we insert a three-mirror ring cavity as mode cleaner in the fundamental frequency optical path, the second harmonic optical path, and the local oscillator optical path of the balanced homodyne detection part of the experimental system. In addition, in the above preparation experiment system for continuous variable high-power bright squeezed state light field, all-optical resonant cavities and the relative phase of the light field are locked by Pound-Drever-Hall technology. The experimental preparation process of the continuous variable high-power bright squeezed state light field is as follows: the laser field output from the high-power single-frequency Nd:YVO₄ solid-state laser of 1064 nm is divided into two parts by the 90/10 beam splitter. One part, as the local oscillator, is injected into the balanced homodyne detector to amplify the noise power of the squeezed state light field. The other part is divided into two beams with equal optical power by the 50/50 beam splitter. Specifically, one is injected into the flat-concave semi-monolithic standing cavity as the fundamental frequency light to generate the second harmonic light field for pumping the optical parametric amplifier, and the other is injected into the optical parametric amplifier as the seed light to generate the bright squeezed state light

field. In order to obtain a high-power bright squeezed state light field, it is necessary to increase the power of seed light. However, the high-power seed light will cause the intense absorption of high-power bright squeezed state light field in PPKTP crystal, which leads to serious thermal effects. This will bring great challenges to the precise locking of the relative phase of the pump light and the seed light, as well as the stable control of the cavity length of the optical parametric amplifier. Therefore, we design an optical parametric amplifier, which is conducive to the generation of a wide-band squeezed light field.

Results and Discussions Finally, at the analysis frequency of 3 MHz, the bright squeezed state light field with an optical power of 200 μW and squeezing degree of (-10.7 ± 0.2) dB is directly measured (Fig. 2). According to the experimental data and theoretical calculation, the total optical loss during the transmission and detection of the high-power bright squeezed light field is $(9 \pm 0.05)\%$. According to Eq. (2), the escape efficiency of the optical parametric amplifier can be calculated as $(66.7 \pm 0.05)\%$. The optical parametric amplifier's intracavity loss due to the absorption of PPKTP crystal is estimated to be $(5.8 \pm 0.05)\%$ by removing the optical loss introduced by the optical devices and the detection process, which accounts for $(64.4 \pm 0.05)\%$ of the total optical loss. According to Beer-Lambert law, the absorption coefficient of PPKTP crystal under this condition is about $6.0 \times 10^{-2} \text{ cm}^{-1}$. By comparing with the experimental preparation system of the squeezed vacuum state, whose optical parametric amplifier's escape efficiency is 98.34%, and the corresponding absorption coefficient of PPKTP crystal is about $2.1 \times 10^{-4} \text{ cm}^{-1}$, it can be concluded that absorption of PPKTP crystal is the main reason for the increase in intracavity loss and the decrease in escape efficiency.

Conclusions An experimental system for generating continuous variable bright squeezed light with high power is established. The bright squeezed light with the power of 200 μW and quantum noise reduction of (-10.7 ± 0.2) dB is obtained by direct measurement at the analysis frequency of 3 MHz with a seed light power of 500 mW and light power of 145 mW pump (Fig. 2). According to the above experimental data and calculation, the total optical loss of the experimental system after the optical parametric amplifier is $(9 \pm 0.05)\%$, and the intracavity loss introduced by the green light-induced infrared absorption effect is $(5.8 \pm 0.05)\%$, accounting for $(64.4 \pm 0.05)\%$ of the total optical loss. Under these conditions, the absorption coefficient of PPKTP crystal to the high-power bright squeezed light is about $6.0 \times 10^{-2} \text{ cm}^{-1}$, while the absorption coefficient of PPKTP crystal to the squeezed vacuum state is about $2.1 \times 10^{-4} \text{ cm}^{-1}$. The above research results confirm that the optical parametric amplifier's intracavity loss introduced by the green light-induced infrared absorption effect becomes the main factor affecting the quantum noise of bright squeezed light with high power. The research conclusion of this manuscript points out the technical difficulties in the current experimental preparation of high-power bright squeezed state light field and the direction for developing a bright squeezed state light field with a higher power, stronger squeezing, and more stable index.

Key words quantum optics; bright squeezed light field; green light-induced infrared absorption effect; intracavity loss